Nano Research Energy

ISSN 2791-0091 (print); 2790-8119 (online)
https://doi.org/10.26599/NRE.2023.9120084

Review Article

Recent progress on the synthesis and applications of high-entropy alloy catalysts

Xiaoxiao Han[1,2], Lingling Zhang[1,2] (✉), Xiao Wang[1,2], Shuyan Song[1,2] (✉), and Hongjie Zhang[1,2,3] (✉)

[1] *State Key Laboratory of Rare Earth Resource Utilization, Changchun Institute of Applied Chemistry, Changchun 130022, China*
[2] *University of Science and Technology of China, Hefei 230026, China*
[3] *Department of Chemistry, Tsinghua University, Beijing 100084, China*

Received: 1 February 2023 / **Revised:** 10 June 2023 / **Accepted:** 21 June 2023

ABSTRACT

High entropy alloys (HEAs) based on five or more elements have caught worldwide attention due to the excellent properties endowed by their unique structures. Compared with traditional alloys, HEAs have high strength, thermal stability, oxidation resistance, and corrosion resistance. In recent years, the rapid development of HEAs shed light on the designing of new alloy systems. Their mixed multi-metallic sites give rise to a great potential for catalytic applications. In this review, we briefly introduce the phase structures of HEAs and their four core effects. In addition, the latest advances regarding HEAs are systematically summarized, with emphasis on the synthesis methods and catalytic applications, such as thermal-driven catalysis and electrocatalysis. To sum up, the current progress, challenges and future prospects of HEAs are discussed, hoping to provide a valuable route to understand this research field.

KEYWORDS

high entropy alloys, core effects, thermal-driven catalysis, catalysis, synthesis

1 Introduction

Catalysis technology, as the backbone of modern industry, environment and energy, has been the focus of scientific research today, and the development of efficient, inexpensive and stable catalysts is a long-term goal. High entropy alloys (HEAs) have unique high entropy characteristics and surface structure, which have great advantages in the field of catalysis [1]. Generally, the elemental species and ratios of HEAs can be widely adjusted, which leads to an almost continuous distribution of adsorption energy. By adjusting the composition and ratios of elements, the optimal adsorption strength can be obtained, thus maximizing the catalytic activity. In addition, HEAs as catalysts can reduce the usage of noble metals that usually have high catalytic activity, and further improve the applicability of the catalysts. Therefore, the emergence of HEAs holds new promise for the field of catalysis.

Yeh et al. first proposed the notion of HEAs in 2004, revising the design principles of conventional alloys [2, 3]. They hypothesized that the high mixing entropy derived from HEAs was sufficient to overcome the formation enthalpy of the intermetallic compounds, thus preventing the formation of intermetallic compounds and generating a homogenous single-phase solid solution. In general, HEAs are produced by alloying five or more equimolar or near-equimolar high concentrations of major elements to maximize configurational entropy, which allows the composition space of alloys to be further expanded compared with conventional alloys containing only one or two main elements. And the number of phases in HEAs is much less than that determined by the Gibbs phase rule. In particular, there is no single dominant element due to each atom occupying lattice sites randomly, which inhibits phase separation to some extent.

HEAs are usually defined in two ways. One is the entropy-based definition of HEAs, where the total mixing entropy consists of four parts, which include configuration entropy, vibration entropy, electronic entropy and magnetic entropy. Among them, configurational entropy accounts for the largest proportion. In terms of component-based definitions, HEAs usually consist of 5–13 elements with an atomic percentage between 5 and 35 atomic% (at.%). However, when $n \geq 9$ (n is the number of elements), the increase of configurational entropy would slow down, resulting in the number of elements usually maintaining 5–9 in practical applications.

HEAs often exhibit unique properties due to their homogeneous multielement composition, which are known as core effects, including the high-entropy effect, sluggish diffusion effect, severe lattice distortion effect and cocktail effect [4].

(1) High-entropy effect in thermodynamics

The total mixing entropy of HEAs increases with the element species, thus leading to a higher entropy than conventional alloys. In particular, the increase in entropy can reduce the immiscible gap between elements, which will decrease the brittleness of the

© The Author(s) 2023. Published by Tsinghua University Press. The articles published in this open access journal are distributed under the terms of the Creative Commons Attribution 4.0 International License (http://creativecommons.org/licenses/by/4.0/), which permits use, distribution and reproduction in any medium, provided the original work is properly cited.

Address correspondence to Lingling Zhang, zhangll@ciac.ac.cn; Shuyan Song, songsy@ciac.ac.cn; Hongjie Zhang, Hongjie@ciac.ac.cn

materials. And according to the Gibbs free energy equation, high entropy will significantly reduce the Gibbs free energy, which further enhances the stability of the materials.

(2) Sluggish diffusion effect in kinetics

The sluggish diffusion effect refers to the relatively slow diffusion of elements in the diffusion process of HEAs compared with conventional alloys. The local environment of each atom is different in HEAs due to the randomization of the occupied lattice sites. In the process of atomic diffusion, when an atom hops into a low-energy site, it will be trapped and unable to return to its original environment; instead, if an atom hops into a high-energy site, it will have a chance to jump back to its original low-energy site due to its instability. In either case, the diffusion rate will decrease. In addition, the increase in packing density will also lead to slow diffusion due to the multiple elements contained in HEAs [5]. The higher diffusion activation energy allows the stability of HEAs to be enhanced and the ability to maintain high ductility, strength and toughness at high temperatures [6, 7].

(3) Lattice distortion effect in structures

The solid solution structures of HEAs contain a variety of elements, which are randomly dispersed throughout the lattice. Due to the large differences in the atomic radii of the elements, the internal structure of the crystals changes, which in turn results in large distortions in the crystals of the alloy and therefore affects the physical and mechanical properties of HEAs. The magnitude of lattice distortion is closely related to the differences in radii between atoms, chemical bonding states, electronic structures and other factors. In addition, the severe lattice distortion effect will lead to the generation of atomic level stresses and ultimately put the atoms in thermodynamically non-equilibrium sites of the lattice. As a result, HEAs have higher potential energy, leading to a lower energy barrier in the catalytic process, which is conducive to improving the reaction performance of HEAs [8, 9].

(4) Cocktail effect on performance

The major elements of HEAs have different properties, and the interaction between the atoms of different elements makes the HEAs exhibit a mixing effect, that is, the cocktail effect [10]. More specifically, the overall properties of HEAs are not only determined by the basic properties of independent elements, but also by the interactions among them. The synergistic effect of multiple elements may give rise to unexpected properties of HEAs and has great application potential.

To date, various HEAs have been developed and shown broad application prospects in catalysis owing to their excellent properties, such as ammonia decomposition reaction, ammonia oxidation reaction, hydrogen evolution reaction [11, 12]. In this review, the phase structure of HEAs was firstly briefly introduced. Then several novel preparation methods related to HEAs and their applications in catalysis were reviewed based on the research achievements, with a view to providing guidance for the further development and application of HEAs in the future.

2 Phase structures of HEAs

HEAs involve a variety of phases, such as solid solutions, intermetallic compounds, amorphous alloys or mixtures of these phases. In general, the solid solution phase is the most widely studied phase structure in HEAs. And there are over 2000 types of intermetallic compounds, including σ, μ, χ, and Laves phases, etc., while the amorphous alloy structures mainly occur during the formation of bulk metallic glasses [13–15]. The phase structures of HEAs play a crucial role in determining their properties [16]. In this paper, we divide the phase structures of HEAs into two main categories based on the number of phases: single-phase HEAs and mixed-phase HEAs.

2.1 Single-phase HEAs

Single-phase HEAs mainly involve three types of Face-centered cubic (FCC), body-centered cubic (BCC) and hexagonal close-packed (HCP) phase [17, 18].

(1) Face-centered cubic

CrMnFeCoNi alloy (Cantor alloy), consisting of equimolar contents of Cr, Mn, Fe, Co and Ni, is a typical HEA with FCC single-phase structure. Due to the excellent strength, ductility and fracture resistance at both room and cryogenic temperatures, Cantor alloy has been extensively studied since it was proposed by British Professor B. Cantor in 2004 [2, 19, 20]. In particular, their properties can be further improved by changing the compositions via adding, replacing, removing elements, or adjusting the proportion of certain elements [21–23]. For example, Chen's group strengthened CrMnFeCoNi HEA by adding different concentrations of Mo [24]. They found that with the increase of Mo content, the yield strength of the alloy gradually increased, while the fracture strain decreased from 50% to 19%. And when the content of Mo reaches 11%, the compressive strength of the alloy is the best, indicating that the addition of Mo can strengthen CrMnFeCoNi HEA.

(2) Body-centered cubic

The BCC phase structure has a coarse stacking structure and more interstitial sites. HEAs with BCC structure are typically composed of refractory metals such as MgTiVCrFe [25], HfNbTaTiZr [26], all of which have excellent strength at high temperatures. For instance, Liaw's group developed the CrMoNbV refractory HEA with BCC phase structure that still has a yield strength of 1062 ± 21 MPa at 1273 K. And even after long annealing treatment at this temperature, the yield strength remains above 1000 MPa [27].

(3) Hexagonal close-packed

Compared with FCC and BCC phase structures, few studies have focused on HEAs with HCP structure [28]. Rare earth elements were considered to be the most likely to form HEAs with HCP structures due to their similar atomic radii and crystal structures, such as YGdTbDyLu [29], HoDyYGdTb [30]. However, rare earth elements usually exhibit poor mechanical properties, and the similar atomic radii result in a lack of solid solution effects. In order to solve these problems, many efforts have been devoted to developing HEAs with HCP structures based on transition metal elements [31]. To date, the direct synthesis of HEAs with HCP single-phase structures remains a challenge, as most elements in the periodic table prefer BCC or FCC structures [32].

2.2 Mixed-phases HEAs

There are many types of mixed-phase structures, such as FCC+BCC, FCC+HCP, BCC+HCP [33–35]. HEAs usually coexist in two or more phases because phase transitions occur between the various solid solution phase structures. For instance, CrMnFeCoNi undergoes a martensitic transition from FCC to HCP phase under high pressure, and CrxMnFeNi HEA would experience a phase transition from FCC to BCC as the Cr content changes, both leading to the presence of mixed-phases in HEAs [36, 37].

More importantly, the blending of multiple phases may

improve the overall properties of HEAs compared with single phases [38]. For example, the NiFeCoCrCu HEA film underwent a phase transition from ductile FCC to hard BCC under ion radiation, and the presence of this mixed-phase structure achieved strong strain-hardening capabilities and large tensile ductility [39]. Therefore, the formation of mixing phases overcomes the strength-ductility trade-off and further optimizes the properties of HEAs, making phase engineering a hotspot of current research [40–42].

Based on the above analysis, the initial phase structure of HEAs cannot be maintained under changing external conditions, which results in the conformational entropy being unable to predict the formation of solid solutions [43]. In order to solve this problem, various parameters have been proposed, such as atomic size mismatch (δ), electronegativity difference ($\Delta\chi$), electron-atom ratio, valence electron concentration (VEC) [44–46]. In general, it is advisable to choose elements with small differences in atomic electronegativity and radii and a high mixing entropy value to reduce the incompatibility among elements, which can facilitate the formation of HEAs with excellent solid solution structures.

3 Synthesis methods of nanosized HEAs

Nanosized HEAs have the advantages of high specific surface area and multiple active sites, and are expected to be used as catalysts. Therefore, the synthesis of nanosized HEAs is very important [47–50]. Many facile and controllable methods have been developed to obtain nanoscale HEAs with larger surface areas and more active sites [51, 52]. The next section will focus on several novel approaches in recent years.

3.1 Carbothermal shock synthesis

Carbon thermal shock (CTS) is a new method to prepare HEA NPs by flash heating and cooling, which was developed by Li's team [53]. This method allows to alloy eight immiscible elements into single-phase solid solution nanoparticles (NPs) (Figs. 1(a) and 1(b)). At first, the precursors of various metal salts were mixed into a solution and then loaded onto a conductive carbon support. After drying, they employed flash heating and cooling, where the temperature was about 2000 K at momentary timespans. According to Eq. (1), these metal salts decomposed into small liquid droplets, and the subsequent rapid cooling crystallized these liquid droplets into homogeneous HEA NPs.

$$MCl_xH_y \rightarrow M(liq) + gases\uparrow \quad (1)$$

The rapid fission and fusion of the particles were driven by the high temperature and the catalytic activity of liquid metals. In addition, rapid cooling facilitated the kinetic control of the thermodynamic mixing state, resulting in the homogeneous distribution of HEA NPs on the carbon support (Figs. 1(c) and 1(d)).

By tuning the carbon thermal shock parameters, such as

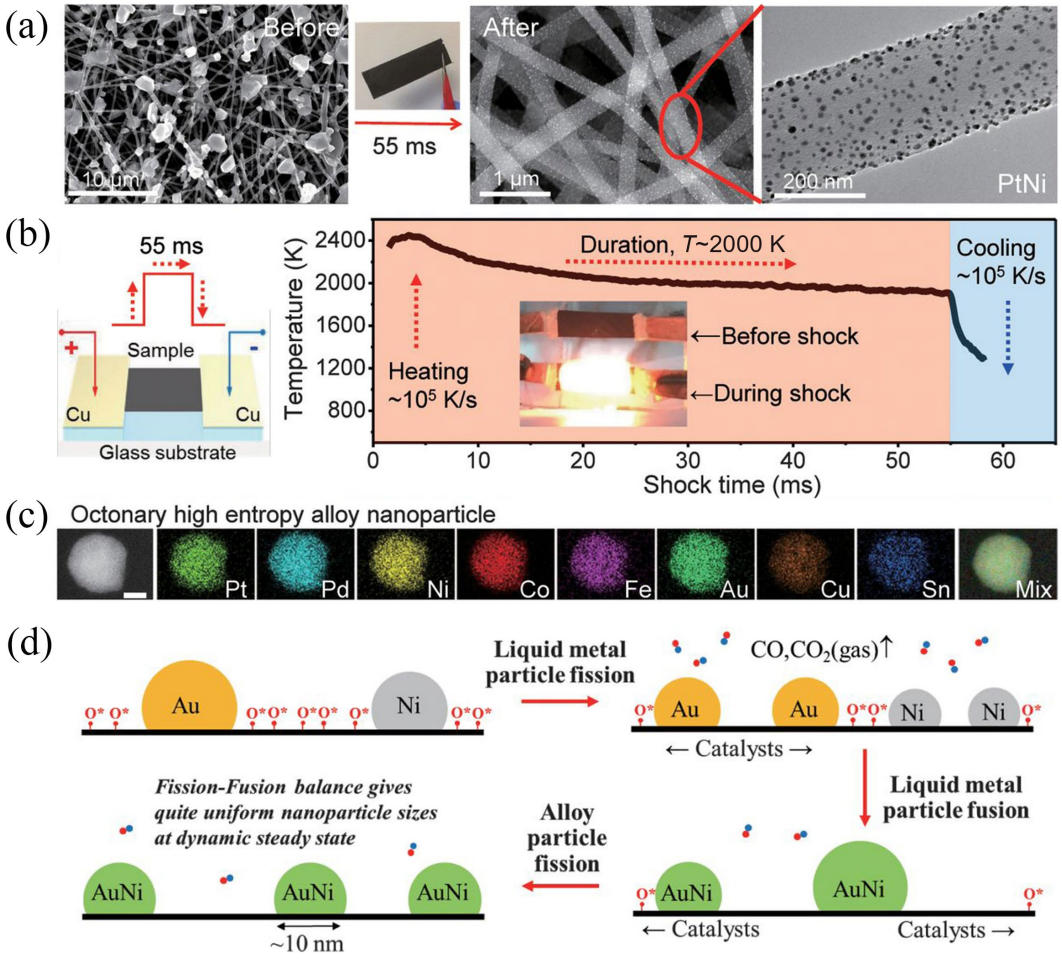


Figure 1 (a) Microscopy images of precursor supported on the carbon nanofiber (CNF) before and after CTS. (b) Sample preparation and the temperature evolution under CTS during 55 ms. (c) Elemental maps of HEA NPs. (d) Schematic illustration of particle fission/fusion mechanism to synthesize HEA-NPs. Reproduced with permission from Ref. [53], © Yao, Y. G., et al. 2018.

substrate, temperature, shock duration, heating/cooling rate, HEAs with specific chemical composition and phase structure can be obtained. Although high temperatures are required for this CTS strategy, the aggregation of NPs can be avoided, leading to a stable and homogeneous distribution on the carbon support. And this method is conducive to the high-rate and high-volume production of HEAs. However, since the carbon support serves not only as catalyst support but also as heating elements, this method is limited to the selection of conductive catalyst supports.

3.2 Fast moving bed pyrolysis synthesis (FMBP)

FMBP strategy overcomes the limitations of supports, which enables to synthesize HEA NPs uniformly dispersed on various granular supports, such as carbon materials, γ-Al_2O_3 and zeolite (Figs. 2(a)–2(d)) [54]. Zhang's group successfully employed this strategy to synthesize ultra-small homogeneous HEA NPs including up to 10 dissimilar elements (Mn, Co, Ni, Cu, Rh, Pd, Sn, Ir, Pt, Au). And the elemental maps showed that each element was homogeneously distributed in the HEA NPs with no phase separation occurring. The conventional fixed bed pyrolysis (FBP) process was to conduct reductive pyrolysis by programmed heating after wet impregnation, which usually led to large nuclei radius and phase separation. In contrast, this FMBP strategy allowed the metal precursors to reach a high temperature of 923 K within 5 s, ensuring the simultaneous pyrolysis of all metal precursors, which led to a high degree of monomer saturation and further facilitated the aggregation of smaller nuclei to form HEA NPs without phase separation. In addition, reasonable temperature, annealing time and reduction rates are the keys to obtaining HEA NPs with a narrow size range.

Although this strategy expands the range of available supports, it is also a demanding preparation process and requires highly specialized equipment. Therefore, it remains important to find more simple and mild preparation methods.

3.3 Dealloying

Dealloying usually employs electrochemical methods to dissolve several unstable metallic elements in precursor alloys, which is an effective way to synthesize nano-porous HEAs. HEAs prepared by this technique typically have a hierarchical structure with large specific surface areas, which can effectively reduce the transport paths of mass and charge, resulting in the improvement of catalytic efficiency [55]. For example, Fujita et al. synthesized FCC phase nano-porous ultra-high-entropy alloys (np-UHEAs) containing up to 14 metal elements (Al, Ag, Au, Co, Cu, Fe, Ir, Mo, Ni, Pd, Pt, Rh, Ru, and Ti) by dealloying technology, which exhibited excellent HER and OER catalytic properties under acidic condition (Fig. 3(a)) [56]. They obtained the alloy ribbons by arc melting followed by re-melting of the ingots. Subsequently, they treated these initial samples in a NaOH solution to leach out Al metal, resulting in the formation of np-UHEAs with elements distributed uniformly.

3.4 Solvothermal synthesis

The solvothermal method is developed based on hydrothermal

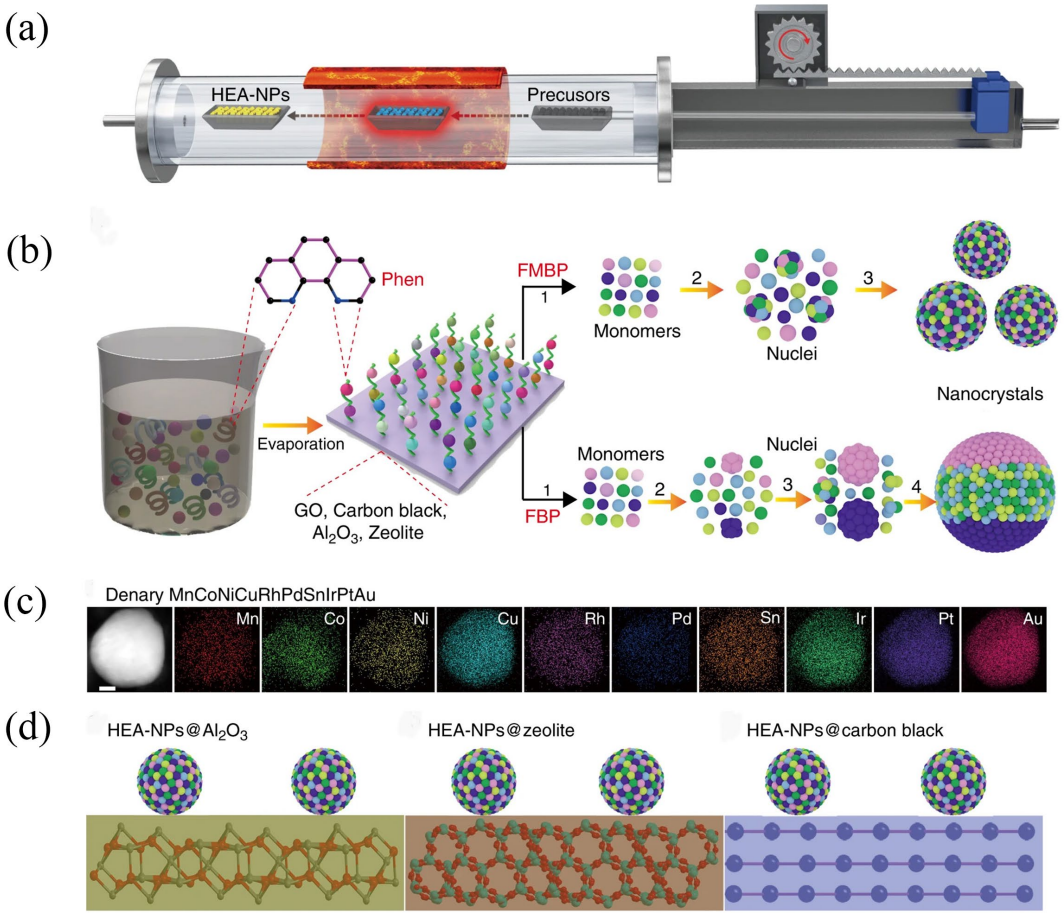


Figure 2 (a) The experimental setup of FMBP. (b) The synthesis of HEA NPs via FMBP and FBP, respectively. (c) Elemental maps of HEA NPs. (d) HEA NPs supported on various supports. Reproduced with permission from Ref. [54], © Gao, S. J., et al. 2020.

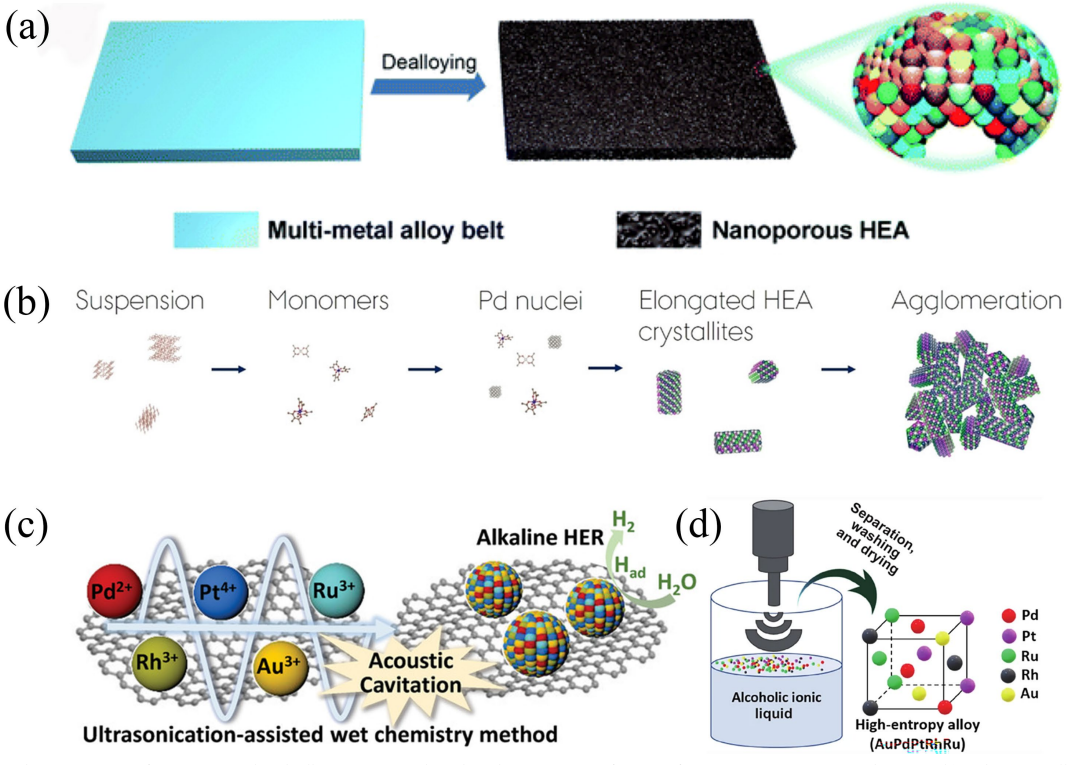


Figure 3 (a) Synthesis process of np-UHEAs by dealloying. Reproduced with permission from Ref. [56], © Cai, Z. X., et al. 2021. (b) Schematic illustration of the formation mechanism for PtIrPdRhRu HEA NPs by solvothermal method. Reproduced with permission from Ref. [57], © Wiley-VCH GmbH 2020. (c) and (d) The synthesis process of HEA-NPs/carbon catalysts and AuPdPtRhRu. Reproduced with permission from Ref. [58], © Wiley-VCH Verlag GmbH & Co. KGaA, Weinheim 2019; Ref. [59], © Tsinghua University Press and Springer-Verlag GmbH Germany, part of Springer Nature 2021.

synthesis and can be used to synthesize HEA NPs in a non-aqueous solvent closed system under high pressure and temperature. In particular, this strategy has the advantage of effectively controlling the grain size, morphology and phase structure of HEA NPs [55]. Iversen et al. used metal acetylacetonate as precursors to synthesize Pt-Ir-Pd-Rh-Ru HEA NPs by autocatalysis under benign low-temperature solvothermal conditions, in which the reaction temperature was as low as 200 ℃ (Fig. 3(b)) [57]. It was demonstrated that the formation of HEA NPs stemmed from the initial Pd nuclei, which autocatalyzed the reduction of other metal ions on the (111) face of the nanocrystals. And the autocatalytic activity remained constant throughout the reaction. In particular, such an autocatalytic process was kinetically driven and may not only be limited to the synthesis of thermodynamically stable HEAs, which provides a possible route for the preparation of more HEAs with specific properties.

3.5 Ultrasound-assisted wet chemical synthesis

Ultrasonication-assisted wet chemistry is a novel and facile method for the preparation of HEA NPs. In the process of ultrasound irradiation, when the ultrasonic wave reaches a certain value, tiny bubbles will form, then grow and eventually collapse, which is called acoustic cavitation. This acoustic cavitation results in the immediate generation of ultra-high temperature and high pressure around 5000 ℃ and 2000 atm in local microscopic regions, thus facilitating the formation of HEA NPs. Notably, the preparation process can be carried out at room temperature, and HEA NPs loaded on various substrates can be synthesized.

For example, Dai's group synthesize PtAuPdRhRu HEA NPs by equimolar amounts of K_2PdCl_4, $HAuCl_4$, H_2PtCl_6, $RuCl_3$, and $RhCl_3$ as precursors, which exhibited superior activity for hydrogen evolution reaction under alkaline conditions (Fig. 3(c)) [58]. With intense ultrasound irradiation, a large amount of energy generated by acoustic cavitation is released instantaneously. This leads to the co-reduction of Pt^{4+}, Au^{3+}, Pd^{2+}, Rh^{3+}, and Ru^{3+} ions under ambient conditions, which results in the formation of amorphous HEA NPs on carbon supports. However, the resulting NPs exhibited a two-phase microstructure, which required further calcination at 700 ℃ under N_2 atmosphere to obtain single-phase HEA NPs.

In order to develop single-step ultrasound-driven pathway, Dai et al. used alcoholic ionic liquids (AIL) as the reaction media. Because of the intrinsic reducing ability of the hydroxyl group, the reduction of metal species and the stability of HEA NPs can be achieved simultaneously (Fig. 3(d)) [59]. Therefore, the subsequent calcination process under N_2 atmosphere can be eliminated. In addition, the obtained nano-catalysts exhibited excellent catalytic performance for selective hydrogenation of phenols. This improved method offers further possibilities for the sustainable synthesis of HEA NPs.

With the emergence of more and more synthetic methods, the types of HEAs are gradually enriched. Therefore, the application potential of HEAs is gradually being further developed. Next, we will focus on the latest progress of them in the field of catalysis.

4 Application of HEAs in catalytic reactions

At present, HEAs-related catalytic reactions can be mainly divided into two categories, one is thermal-driven catalysis, which includes ammonia decomposition reactions, ethanol oxidation reactions, methanol oxidation reactions, CO oxidation reactions, and the other is electrocatalysis, which mainly includes hydrogen evolution reaction (HER), oxygen evolution reaction (OER), carbon dioxide reduction reaction (CO_2RR) and so on [60]. Next,

we will introduce the application of HEAs in these reactions in detail.

4.1 Thermal-driven catalysis

4.1.1 *Ammonia decomposition reaction*

Ammonia possesses a high weight hydrogen density of 17.8 wt.% and a theoretical hydrogen conversion efficiency of 89.3% [61]. In addition, the storage and transportation of ammonia is also a relatively mature technology. Therefore, ammonia decomposition is a promising way to obtain pure hydrogen. The noble metal Ru is an efficient catalyst for this reaction, but it is limited by the high price and scarce resources. Subsequently, the Co-Mo binary system was further developed, but due to the limitation of the immiscible gap between Co and Mo elements, it was not conducive to the continuous adjustment of the element ratio and is prone to phase separation. The entropy-induced stabilization in HEAs overcomes this difficulty and enables continuous tunability of elemental ratios. Compared with the conventional Co-Mo binary system, HEA catalysts exhibit superior catalytic performance.

For example, Wang's group successfully prepared $Co_xMo_yFe_{10}Ni_{10}Cu_{10}$ ($x + y = 70$) HEA NPs and they found that most HEA-Co_xMo_y catalysts had better performance than bimetallic Co-Mo and monometallic Ru. By adjusting the amounts of precursors, the atomic ratios of Co and Mo were controlled at 15/55, 25/45, 35/35, 45/25 and 55/15, respectively [62]. $Co_{25}Mo_{45}Fe_{10}Ni_{10}Cu_{10}$ achieved a mass-specific rate of 22.1 $g_{NH_3} \cdot g_{metals}^{-1} \cdot h^{-1}$ at 500 ℃ under 5 vol.% NH_3 (Figs. 4(a) and 4(b)). Moreover, the HEA-Co_xMo_y catalysts exhibited high stability during ammonia decomposition (Fig. 4(c)).

Then, Wang et al. further studied the mechanism of volcanic-type behavior of catalysts with different Co/Mo ratios. According to the Sabatier principle, the catalyst with high Co content has weak binding with N, resulting in relatively high barriers to dehydrogenation kinetics (NH_3 → $*NH_2$ → *NH → *N). In contrast, the catalyst with high Mo content has strong binding ability to N, resulting in poor desorption of N_2 from the surface ($2*N \rightarrow N_2$) (Fig. 4(d)). Therefore, by optimizing the Co/Mo ratio, the binding ability of the catalyst to N can be adjusted to obtain the best ammonia decomposition performance. In addition, different ammonia concentrations also have certain effects on the adjustment of the Co/Mo ratio. With continuous adjustment of the Co/Mo ratio in HEAs, catalysts can be prepared to match different NH_3 concentrations, thus exhibiting the best ammonia decomposition performance (Fig. 4(e)).

4.1.2 *Ammonia oxidation reaction*

A crucial step in the industrial synthesis of nitric acid is the formation of NO_x (NO + NO_2) by ammonia oxidation, in which N_2 and N_2O by-products are inevitably formed. Although many efforts have been made in the development of ammonia oxidation catalysts, PtPdRh-based multimetallic catalysts are still predominantly used in industrial applications. In addition, the ammonia oxidation reaction is usually carried out at high temperatures, which makes it difficult to achieve high stability. Therefore, it is very important to reduce the amounts of noble metals in the catalyst and maintain its high stability.

Hu's group prepared PtPdRhRuCe HEA-NPs via the CTS method, which reduces the amount of noble metal Pt by introducing Ru and Ce [53]. The HEA NPs achieved approximately 100% ammonia conversion and >99% selectivity

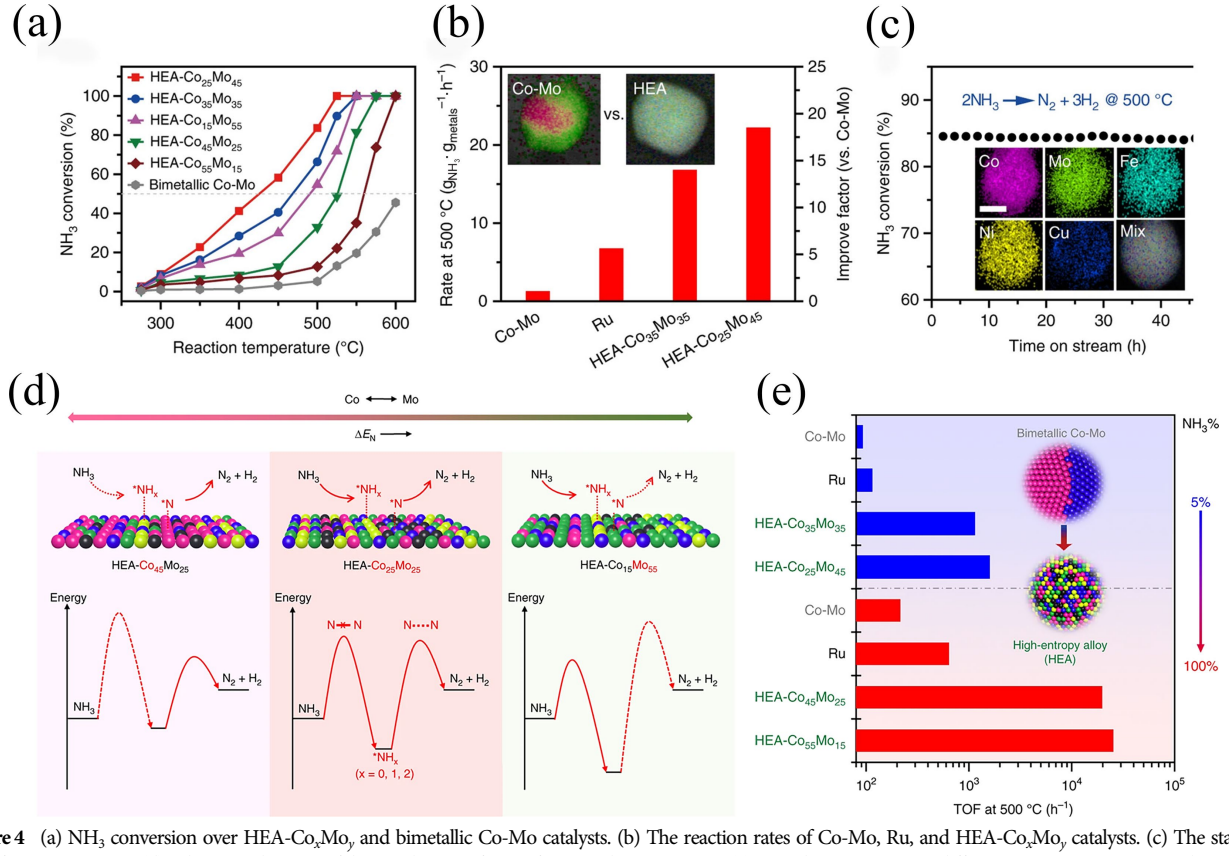


Figure 4 (a) NH_3 conversion over HEA-Co_xMo_y and bimetallic Co-Mo catalysts. (b) The reaction rates of Co-Mo, Ru, and HEA-Co_xMo_y catalysts. (c) The stability test of HEA-$Co_{25}Mo_{45}$. (d) Schematic diagram of the rate-limiting factors for NH_3 decomposition. (e) NH_3 decomposition at different concentrations. Reproduced with permission from Ref. [62], © Xie, P. F., et al. 2019.

for NO_x ($NO+NO_2$) at an operation temperature of 700 ℃. In contrast, the PtPdRhRuCe MMNPs prepared by wet impregnation had a very low NO_x selectivity, with most of the products being N_2. STEM elemental maps showed that the catalysts obtained by the wet impregnation method had a phase-separated heterostructure. Instead, the HEA NPs prepared by the CTS method were highly homogeneous, which may be the main reason for their catalyst enhancement. In addition, due to the high entropic nature of HEAs, the catalysts exhibited excellent stability with no decrease in selectivity and conversion when operated continuously at 700 ℃ for 30 h (Figs. 5(a)–5(e)).

4.1.3 *CO oxidation reaction*

Carbon monoxide is one of the most common toxic and harmful pollutants in the atmosphere. It is colorless and odorless, which poses a serious threat to the ecological environment and human health. In recent years, the removal of CO from the atmosphere has received extensive attention, and catalytic oxidation is one of the most important methods. Therefore, the development of CO oxidation catalysts has always been the research hotspot. HEAs usually have excellent thermal stability and can reduce the amounts of noble metals, which has great application potential for CO oxidation reaction.

Qiu's group synthesized senary nano-porous AlNiCuPtPdAu HEA NPs (np-HEAs), which have a naturally formed thin oxide layer of spinel γ-Al_2O_3 [63]. They found that np-HEAs with the oxide coating showed slight coarsening and excellent thermal stability under high temperatures, while np-HEAs with metal oxide coating removed by acid leaching showed severe coarsening. In addition, np-AlPt without oxide coating showed higher coarsening than np-HEAs (with the coating etched off) under the same conditions. As a result, the np-HEAs exhibited optimal catalytic performance for CO oxidation due to the synergistic effect between the metal oxide coating and the HEAs core (Figs. 6(a) and 6(b)). The metal oxide coating may facilitate the dissociation of O_2 into atomic oxygen, thus promoting the CO oxidation reaction process.

4.1.4 *CO_2 hydrogenation reaction*

With the massive use of fossil fuels, global warming has become a major environmental issue, and CO_2 is one of the main reasons for the greenhouse effect. CO_2 hydrogenation reaction is one of the main routes to reduce the amount of CO_2 in the atmosphere, which can convert it into energy products to achieve carbon neutrality. Recently, HEAs have also exhibited great application potential in the field of CO_2 hydrogenation due to their extremely strong durability.

Mori's group synthesized CoNiCuRuPd HEA NPs supported by TiO_2, and investigated the catalytic activity during CO_2 hydrogenation with Pd/TiO_2 as a comparison sample. CoNiCuRuPd HEA NPs showed excellent catalytic activity for the hydrogenation of CO_2, and the main products were CO and CH_4; On the contrary, Pd/TiO_2 showed relatively low catalytic activity, and the main product was CO (Figs. 7(a)–7(c)) [64]. Due to the desorption characteristics of CO molecules at metal sites with different binding strengths, the two catalysts have different selectivity for CO and CH_4. Specifically, the adsorption sites on $CoNiCuRuPd/TiO_2$ are electron-rich compared with Pd/TiO_2. And the strong interaction delays the desorption of CO intermediates, which in turn promotes the formation of CH_4 and therefore increases the efficiency of the CO_2 hydrogenation reaction.

4.2 Application of HEAs in electrocatalysis

Electrocatalysis is also an important part in the field of catalysis. Electrocatalytic reactions mainly include hydrogen evolution reaction (HER), oxygen evolution reaction (OER), carbon dioxide reduction reaction (CO_2RR), alcohol oxidation reaction (AOR), nitrogen reduction reaction (NRR). Currently, the efficient catalysts for these reactions are mainly precious-metal-based catalysts, which are limited by their high price and scarce resources. In order to solve this problem, transition metal-based catalysts have been greatly developed, but their catalytic efficiency is still insufficient.

HEAs can reduce the amounts of noble metals and achieve high activity due to the variety of constituent elements. In addition, the high specific surface area, multiple active sites and nano-size effect of HEA NPs can further increase their application potential. Therefore, the application of HEAs in electrocatalysis has also attracted widespread interest.

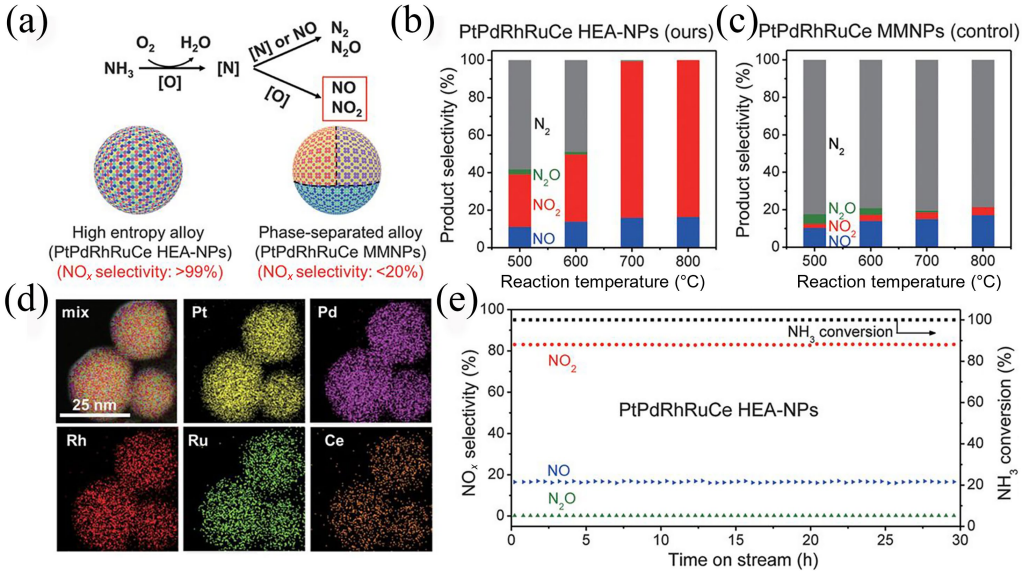


Figure 5 (a) Schematic diagram of the ammonia oxidation reaction. (b) and (c) The product distribution and NH_3 conversion with temperature for PtPdRhRuCe HEA-NPs and PtPdRhRuCe MMNPs, respectively. (d) STEM elemental maps for PtPdRhRuCe HEA-NPs. (e) Catalytic performance of PtPdRhRuCe HEA-NPs at 700 °C as a function of time. Reproduced with permission from Ref. [53], © Yao, Y. G., et al. 2018.

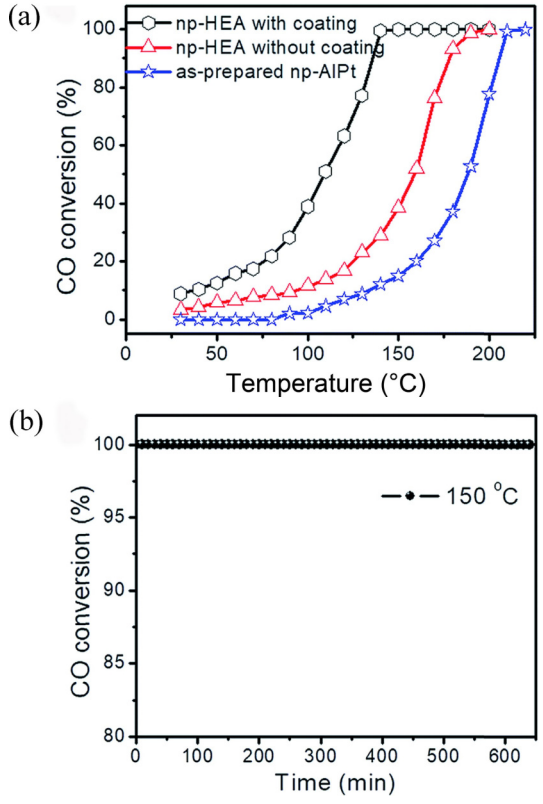


Figure 6 (a) The CO conversion over np-HEA with coating, np-HEA without coating, and as-prepared np-AlPt. (b) The cycling stability of np-HEA with oxide coating. Reproduced with permission from Ref. [63], © The Royal Society of Chemistry 2019.

4.2.1 *Application of HEAs in HER*

Hydrogen is a clean energy source with high energy density. Due to the green and efficient nature, electrolysis of water is one of the most promising methods for producing hydrogen [65]. The noble metal platinum is a highly efficient catalyst for HER and the reaction activity under acidic conditions is typically 2–3 orders of magnitude higher than under basic/neutral conditions. However, the disadvantages of high cost and poor stability make it difficult to apply on a large scale. Therefore, it is essential to develop low-cost, earth-abundant and highly efficient HER catalysts. Unlike conventional metal-based catalysts, HEAs have many excellent properties such as high mechanical strength and high thermal stability. Recently, the application of HEAs in water electrolysis has attracted wide attention.

Lai's group found that Pd can effectively promote HER under alkaline conditions [66]. Recently, they synthesized Pt-free PdFeCoNiCu HEA NPs at low temperature, and then combined with Ketjen Black to obtain PdFeCoNiCu/C catalyst [67]. PdFeCoNiCu/C exhibited excellent alkaline HER catalytic performance for HER compared with Pt/C and Pd/C. Specifically, the overpotential of PdFeCoNiCu/C was only 18 mV at a current density of 10 mA·cm^{-2}, while Pt/C and Pd/C were 91 and 418 mV, respectively. And the mass activity of PdFeCoNiCu/C was 6.51 A·mg$_{Pd}^{-1}$ at –0.07 V vs. RHE, much higher than that of Pt/C. Meanwhile, the Tafel slope was as low as 39 mV·dec^{-1} (Figs. 8(a)–8(e)). In addition, the activity of the catalyst remained unchanged and the carbon material did not detach from the HEA NPs during the 15-day cycling stability test.

They further explored the reasons for this superior performance and found that the five metal elements in PdFeCoNiCu/C play a synergistic role in optimizing the electronic environment. Specifically, Pd and Co were the main active sites for H_2 production and initial water splitting, while Ni, Fe and Cu facilitated electron transfer and optimized the binding energy of the H_2 intermediates.

Similarly, Lang et al. prepared nanoporous CuAlNiMoFe electrodes, in which CuNiMoFe HEAs were formed *in situ* at the CuAlNiMoFe precipitates [68]. The surface HEA provides bifunctional electrocatalytic sites, which enhance the kinetics for water dissociation and the adsorption/desorption of reactive hydrogen intermediates. In addition, the hierarchical nanoporous Cu scaffolds promote electron transfer/mass transport. Therefore, the nanoporous CuAlNiMoFe electrodes exhibited excellent catalytic performance in nonacidic media, reaching current densities of ≈1840 and ≈100 mA·cm^{-2} at overpotentials of –240 mV in KOH and –183 mV in pH 7 buffer electrolytes, respectively. Besides, the nano-porous CuAlNiMoFe electrodes exhibit excellent cycling stability.

4.2.2 *Application of HEAs in OER*

Compared with HER, the kinetics of OER is much slower due to the transfer of four protons and electrons and the existence of a large number of intermediates, which leads to the electrolysis efficiency of water splitting being slow. Although RuO_2 and IrO_2 possess excellent OER catalytic activity, they suffer from high costs, low reserves, and poor stability. Therefore, it is crucial to develop cheap, efficient and stable OER catalysts to further improve catalytic efficiency [69].

Qiu's group synthesized np-AlNiCoFeX (X = Mo, Nb, Cr) via a top-down strategy. The overpotential of np-AlNiFeCoMo was 240 mV at a current density of 10 mA·cm^{-2} and the Tafel slope was 46 mV·dec^{-1} [70]. In addition, the electrochemical impedance spectra (EIS) showed that this catalyst possesses low electrode impedance, indicating a high charge transfer efficiency. They further investigated the reasons for the increase in OER activity, and found that the addition of Mo increased the electron transfer effect and changed the electronic state of the catalyst, resulting in the optimal adsorption of O* on the oxide surface. In addition, the doping of Mo, Nb and Cr tends to be in a high formal oxidation state, which is conducive to proton migration to O at the Ni (Co) site. And the larger Mo atom will generate compressive strain that leads to weaker Ni-O chemisorption. Therefore, the np-AlNiCoFeX (X = Mo, Nb, Cr) exhibited high activities for OER.

4.2.3 *Application of HEAs in AOR*

Alcohol oxidation reaction (AOR) is the anode reaction of direct alcohol fuel cells, which can be mainly divided into methanol oxidation (MOR) and ethanol oxidation (EOR). It is well known that methanol and ethanol have the advantages of high energy storage efficiency and ease of transport and storage. In recent years, direct alcohol fuel cells have attracted a lot of attention for sustainable electricity supply, which uses methanol and ethanol as fuels. At present, the highly active catalyst for alcohol oxidation reactions is still Pt, so it is crucial to find other low-cost and efficient catalysts. The lower-cost Pd has the same crystal structure and similar atomic dimensions as Pt, which makes it a promising alternative to Pt catalysts. Alloying Pd with various other transition metal elements can enhance the activity and thus further improve the efficiency of the alcohol oxidation reaction.

Li et al. prepared quinary PdNiCoCuFe alloy nanotube arrays (NTAs) by template-assisted electrodeposition [71]. The unique

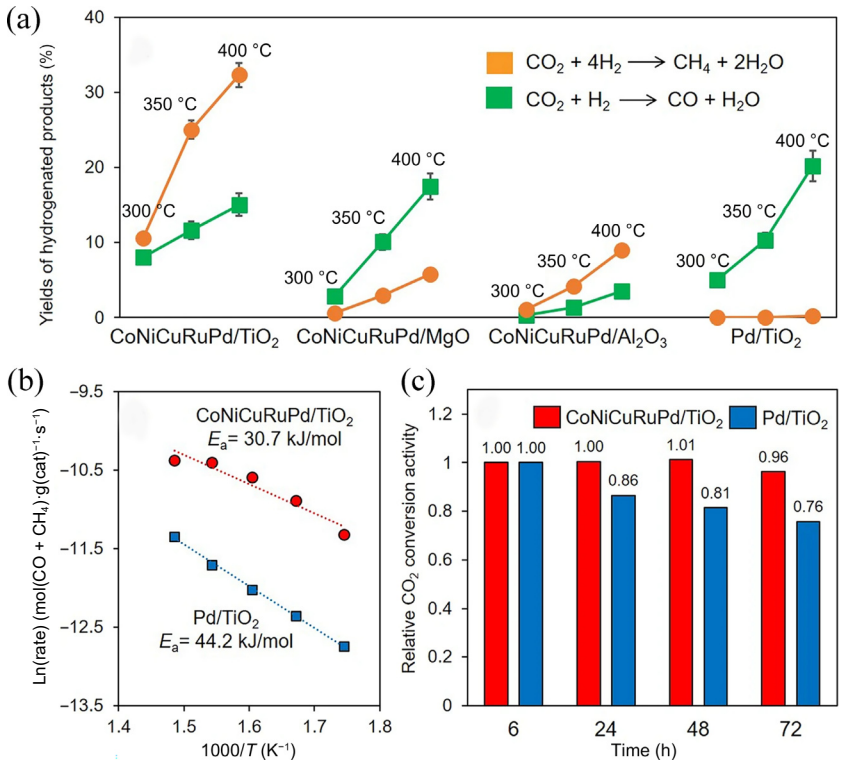


Figure 7 (a) Yields of CH_4 and CO over various catalysts. (b) Arrhenius plots of CoNiCuRuPd/TiO_2 and Pd/TiO_2. (c) The durability of CoNiCuRuPd/TiO_2 and Pd/TiO_2. Reproduced with permission from Ref. [64], © Mori, K., et al. 2019.

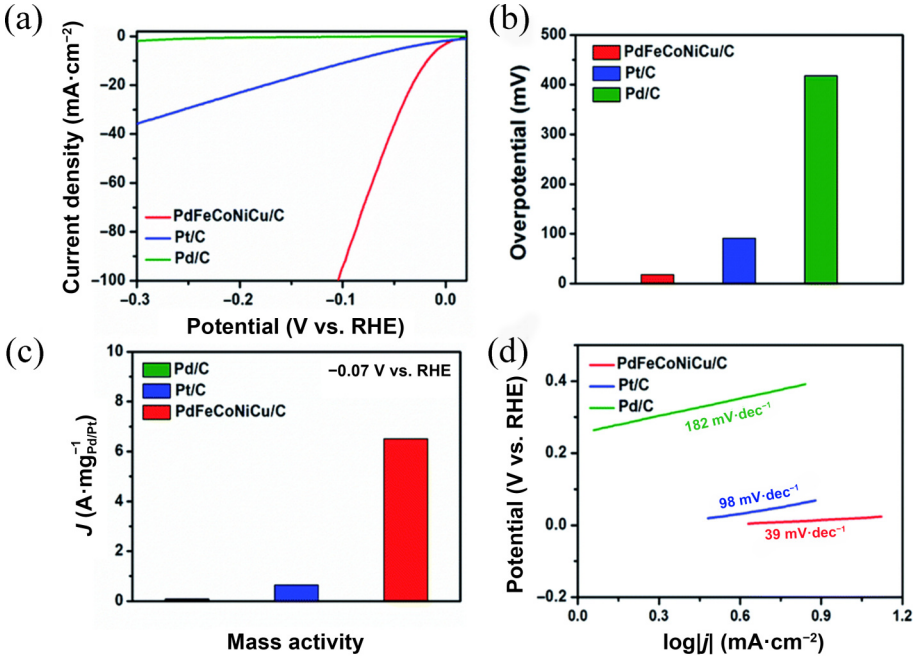


Figure 8 (a)–(c) The Current density, overpotential and mass activity of PdFeCoNiCu/C, Pt/C, Pd/C. (d) The corresponding Tafel curves. (e) HER polarization curves before and after 10,000 CV cycles. (f) The galvanostatic measurement of FeCoNiCu/C. Reproduced with permission from Ref. [67], © The Royal Society of Chemistry 2021.

hollow nanotube structure endowed the PdNiCoCuFe catalyst with more excellent nature properties, such as high specific surface area and high mass transfer efficiency. The specific peak current density of PdNiCoCuFe alloy NTAs in forward scanning was about twice that of Pd NTAs, and the onset potential of forward anodic wave was lower, demonstrating superior electrocatalytic performance. Meanwhile, this catalyst exhibited high cycle stability and strong resistance to the poisoning of carbonaceous species. The enhanced electrocatalytic activity can be attributed to the synergistic interaction between different metal elements, the electronic effects associated with alloys and the unique hollow structure. Specifically, the strong electronic interactions between Pd, Ni, Co, Cu and Fe atoms significantly changed the electronic states of Pd atoms, resulting in excellent electrocatalytic activity of PdNiCoCuFe alloy NTAs and strong resistance to poisoning of carbonaceous species. And the PdNiCoCuFe alloy NTAs can

significantly reduce the adsorption strength of CO on their surface, thus facilitating the removal of CO and providing stronger resistance to CO poisoning. Similarly, the $Pt_{18}Ni_{26}Fe_{15}Co_{14}Cu_{27}$ HEA NPs fabricated by Lai et al. also showed excellent electrocatalytic properties and superior CO anti-poisoning for methanol oxidation reaction in alkaline solutions. The mass activity was up to 15.04 $A{\cdot}mg_{Pt}^{-1}$, approximately 10 times higher than Pt/C catalysts [72].

Ethanol oxidation is a complex 12-electron/12-proton transfer process ($CH_3CH_2OH + 3H_2O = 2CO_2 + 12H^+ + 12e^-$). Wu et al alloyed six platinum-group metals into FCC-phase HEA NPs (PGM-HEA) via a facile wet chemical method [73]. More concretely, the specific activity (mass activity) of PGM-HEA was 2.5 (3.2), 6.1 (9.7), and 12.8 (3.4) times higher than that of the commercial Pd/C, Pd Black, and Pt/C catalysts at 0.45 V, respectively, which exhibited the best EOR catalytic activity. To further understand the origin of this excellent activity, they compared the EOR performance of PGM-HEA with that of each monometallic catalyst and found that the increase in EOR efficiency came from the atomic configuration of solid–solution alloy. Specifically, the six metal elements in PGM-HEA can provide different adsorption sites and effectively promote the oxidation of various intermediates, thus greatly improving the EOR efficiency.

4.2.4 *Application of HEAs in CO_2RR*

CO_2 reduction reaction (CO_2RR) can be a sustainable way to reduce the increase of CO_2 emissions while producing value-added chemicals and fuels. However, this is a complex process that is highly dependent on catalysts and reduction conditions, usually resulting in slow kinetics. The development of highly efficient electrocatalysts is one of the primary approaches to improve the efficiency and selectivity of CO_2 reduction.

Singh's group reported an FCC-structured AuAgPtPdCu HEA catalyst, which exhibited better CO_2RR catalytic performance than monometallic Cu catalysts (Figs. 9(a)–9(d)) [74]. The overall Faradic efficiencies (FE%) were 100% at low potentials, and the main gaseous products were CO, CH_4, C_2H_4, and H_2. Specifically, the Faradic efficiencies of the CO products were ~ 7% at –0.7 V, and that of CH_4 and C_2H_4 were 49.4% and 19.9%, respectively. The redox peak associated with Cu^{2+}/Cu^0 can be seen in the cyclic voltammetry (CV) spectra, indicating that copper plays a major role in the reduction of CO_2. In addition, the AuAgPtPdCu HEA catalyst exhibited excellent long-term stability. Density functional theory (DFT) studies based on free-energy calculations of intermediates are used for further elucidation. The theoretical limiting potential of AuAgPtPdCu HEA was lower than that of pure Cu catalysts, which could be ascribed to the destabilization of the $*OCH_3$ intermediate and the stabilization of the *O intermediate.

4.2.5 *Electrocatalytic nitrogen reduction reaction (NRR)*

The traditional Haber-Bosch process is an effective way to fix nitrogen by converting N_2 to ammonia, but is usually carried out under high temperature and pressure conditions. Electrochemical nitrogen fixation is a gentle and clean route to produce ammonia and holds promise for sustainable ammonia production. However, due to the similar overpotential of nitrogen reduction reactions (NRR) (N_2 (g) + $6H_2O$ (l) + $6e^- \rightarrow 2NH_3$ (aq.) + $6OH^-$ (aq.), E_0=0.092 V vs. reversible hydrogen electrode, RHE) and HER

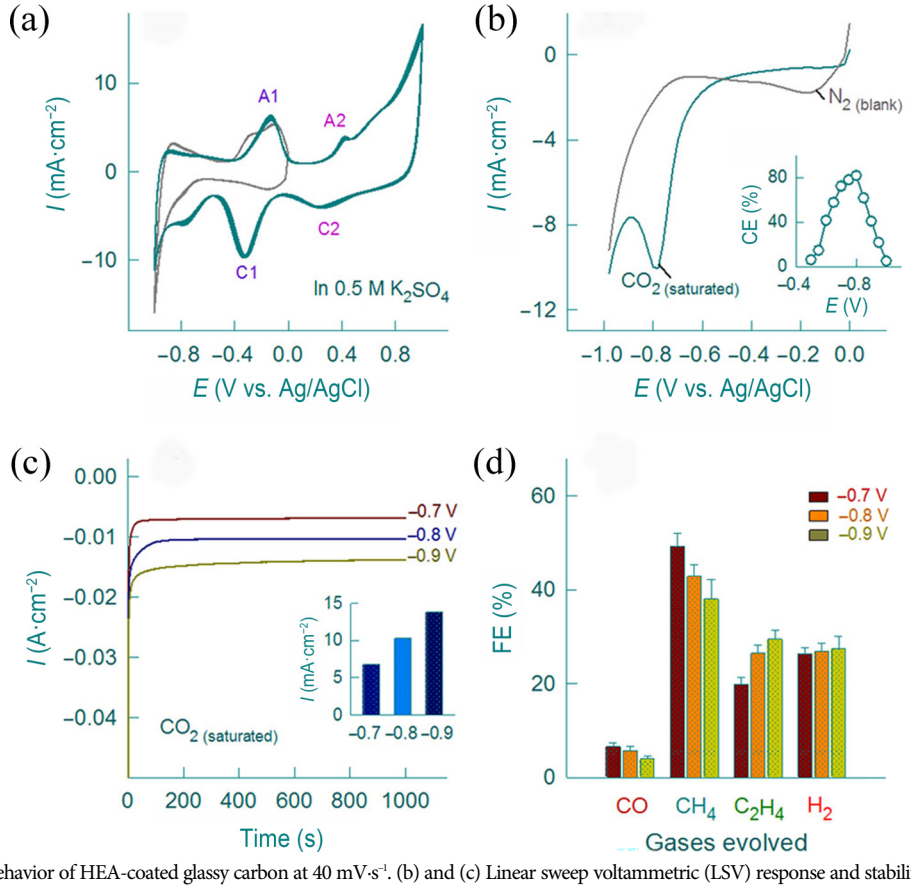


Figure 9 (a) The CV behavior of HEA-coated glassy carbon at 40 $mV{\cdot}s^{-1}$. (b) and (c) Linear sweep voltammetric (LSV) response and stability tests for CO_2RR. (d) Bar diagram for the faradic efficiencies. Reproduced with permission from Ref. [74], © American Chemical Society 2020.

($2H_2O$ (l) + $2e^- \rightarrow H_2$ (g) + $2OH^-$ (aq.), E_0=0 V, vs. RHE), there are competitive reactions in aqueous solutions. The low ammonia yields, high overpotentials and poor stability are still huge challenges for NRR. The stable structure of HEAs allows them to be used in harsh environments and their multi-component form can provide multiple active sites [75]. Therefore, the application of HEAs in NRR has attracted widespread interest.

Lai's group successfully prepared RuFeCoNiCu HEA NPs at low temperatures (≤250 ℃) and ambient pressure [76]. The ammonia yield of this catalyst reached 57.1 $\mu g \cdot h^{-1} \cdot mg_{cat}^{-1}$ (11.4 $\mu g \cdot h^{-1} \cdot cm^{-2}$) at 0.05 V versus RHE in 0.1 M KOH alkaline electrolyte, and the Faraday efficiency was up to 38.5%. In addition, the activity of RuFeCoNiCu remained unchanged after 100 hours of cycling tests. Further theoretical calculations have shown that Fe was the best site for nitrogen adsorption and activation, while the Co-Cu and Ni-Ru couples showed good surface hydrogenation at low potentials. The synergy between the multiple active sites leads to an increase in the final catalytic activity.

Although HEA catalysts have a very promising applications in electrocatalysis, there are still some shortcomings and limitations. Firstly, the catalytic performance is still unsatisfactory, and further development of HEAs with large specific surface area and easily controllable size and shape is still needed. Secondly, electrocatalytic reaction presents a dynamic process involving multiple intermediates, which is accompanied by complex surface redox variation. The multi-component nature of HEAs leads to difficulties in characterizing the adsorption configuration of intermediates and reactants on specific atom. It is difficult to cope with the microscopic active sites and details of the catalytic process. This is also one of the reasons why high entropy electrocatalysts have not achieved theoretical high activity at present. In addition, the complex composition of HEAs is unpredictable. Unreasonable compositions may lead to a lack of performance, which leads to the critical importance of element selection and catalyst design.

Based on the above discussions, HEAs have shown broad application prospects in the field of thermal-driven catalysis and electrocatalysis. The homogeneous mixing of multiple elements in HEAs not only compensated for the shortcomings of single metal but also greatly improve the catalytic efficiency. The summary of various synthesis methods and applications of HEA catalysts is shown in Table 1. Although there have been many related literatures, the application of HEAs in catalysis and the catalytic reaction mechanism need to be further explored.

5 Conclusions and prospects

To date, researchers have developed many methods to synthesize HEAs and further explored their application in catalysis. And the theoretical calculation process helps people understand their mechanism of catalysis. This review systematically summarized the developments of various HEAs, including their classification, synthesis methods and applications in the field of catalysis. In addition, we further analyzed the development direction and difficulties of HEAs in the future.

(1) HEAs are based on five or more elements, and most of them have shown excellent properties due to the four core effects. The wide range of elements allows the use of noble metals to be reduced and provides multiple active sites on the catalytic surface. Although a variety of HEA NPs have been reported, more attention should be paid to developing more facile and scalable synthesis methods. Current methods summarized before typically require strict preparation conditions, such as supports, high temperature, pressure, and complicated equipment. Therefore, how to realize large-scale production of HEA NPs with uniform distribution is crucial. In general, the preparation cost and productivity of catalysts are closely related to their practical applications. Therefore, it is necessary to develop more convenient and green preparation methods to reduce costs and increase productivity, thus facilitating the large-scale synthesis of HEA catalysts.

(2) Although HEAs have shown great application potential in the field of catalysis, their catalytic performance still needs to be further improved. As it is often difficult to simultaneously improve

Table 1 Summary of the synthesis and applications of HEAs-based catalysts

Catalysts	Synthesis methods	Conditions	Supports	Particle size	Application	Ref.
PtPdRhRuCe HEA-NPs	Carbothermal shock (CTS)	~2000 K, 1 atm	Carbon support	~10 nm	Ammonia oxidation reaction	[53]
MnCoNiCuRhPdSnIrPtAu HEA-NPs	Fast moving bed pyrolysis (FMBP)	923 K, Ar	Carbon materials, γ-Al_2O_3 and zeolite	~2 nm	HER	[54]
np-UHEAs (Al, Ag, Au, Co, Cu, Fe, Ir, Mo, Ni, Pd, Pt, Rh, Ru, and Ti)	Dealloying	Room temperature, 1 atm	—	Hierarchical porosity (2–5 nm, 50 nm)	HER, OER	[55]
Pt-Ir-Pd-Rh-Ru HEA NPs	Solvothermal method	473 K, 1 atm	Free-standing	1-3 nm	—	[57]
PtAuPdRhRu HEA NPs	Ultrasound-assisted wet chemical synthesis	Ultrasonic irradiation	Free-standing	3 nm	HER	[58]
$Co_xMo_yFe_{10}Ni_{10}Cu_{10}$ ($x + y = 70$) HEA NPs	Carbothermal shock (CTS)	~2000 K, 1atm	Carbon support	~22 nm	ammonia decomposition reactions	[61]
AlNiCuPtPdAu HEA NPs	Dealloying	Room temperature, 1 atm	—	Ligament sizes of ~2-3 nm	CO oxidation reaction, HER, ORR	[63]
TiO_2-supported CoNiCuRuPd HEA NPs	Hydrogen spillover-driven synthesis	676 K, H_2 reduction	TiO_2	1.9 nm	CO_2 hydrogenation reaction	[64]
PdFeCoNiCu HEA NPs	One-pot oil phase synthesis	493 K, 1 atm	Free-standing	34 nm	HER	[67]
$Pt_{18}Ni_{26}Fe_{15}Co_{14}Cu_{27}$ HEA NPs	One-pot oil phase synthesis	493 K, 1 atm	Free-standing	~3.4 nm	HER, MOR	[72]
PGM-HEA (Ru, Rh, Pd, Os, Ir, and Pt)	Facile wet-chemistry method	503 K, 1 atm	Free-standing	3.1±0.6 nm	EOR	[73]
RuFeCoNiCu HEA NPs	One-pot oil phase synthesis	493 K, 1 atm	Free-standing	~16 nm	NRR	[76]

the activity and selectivity of catalysts, efforts should also be made to further design HEAs with different physical and chemical properties. To solve these problems, we can further optimize the catalytic performance of HEAs by tuning their size, morphology, strain and crystal structure (such as phase structure, phase compositions).

(3) In addition, further comprehensive studies and clarifications are needed to understand the structure-performance relationships of HEAs. *In situ* characterizations and high-precision simulations still need to be further developed in the future, with a view to providing some guidance for catalyst design.

(4) More importantly, the identification of active centers is a key focus in metal catalysis research, which determines the design and improvement of catalysts. The multiple atomic combinations of HEAs make it difficult to elucidate the true active centers by investigation of one or two models. DFT calculation is a powerful tool for the identification of active centers, which can screen out possible active sites according to previous studies, and then further calculate the variation of adsorption free energy towards key intermediates and reactants. In addition, possible active sites can be further validated by removing or replacing an element to compare the effect on the catalysts. However, it is still difficult to determine the active sites of HEAs at present, and more efforts are still needed in the future.

(5) Another important problem is to find the appropriate HEAs composition in the vast element composition space. The rational selection of compositions is very important for the preparation of HEAs with high catalytic activity. We can start with the selection of the active elements based on the reaction, and then select other elements according to the electronic structure of HEAs. In addition, the compatibility between the elements should be considered, combining various physical and chemical parameters such as atomic radius, electronegativity, valence electron concentration, mixing enthalpy and mixing entropy for element selection. High-throughput calculations and screening are effective methods for finding suitable HEAs compositions in the vast element composition space, but these computational methods are still in the preliminary stage of exploration and need to be further explored [77, 78].

All in all, the development of HEAs is still in its infancy, and the component design, synthesis methods and application potentials should be developed in-depth.

Acknowledgements

This work was supported by the financial aid from the National Science and Technology Major Project of China (No. 2021YFB3500700), and National Natural Science Foundation of China (Nos. 22020102003 and 22025506).

Declaration of conflicting interests

The authors declare no conflicting interests regarding the content of this article.

References

[1] Tomboc, G. M.; Kwon, T.; Joo, J.; Lee, K. High entropy alloy electrocatalysts: a critical assessment of fabrication and performance. *J. Mater. Chem. A* **2020**, *8*, 14844–14862.

[2] Yeh, J. W.; Chen, S. K.; Lin, S. J.; Gan, J. Y.; Chin, T. S.; Shun, T. T.; Tsau, C. H.; Chang, S. Y. Nanostructured high-entropy alloys with multiple principal elements: Novel alloy design concepts and outcomes. *Adv. Eng. Mater.* **2004**, *6*, 299–303.

[3] Cantor, B. Multicomponent high-entropy Cantor alloys. *Prog. Mater. Sci.* **2021**, *120*, 100754.

[4] Yeh, J. W. Recent progress in high-entropy alloys. *Ann. Chim. Sci. Mat.* **2006**, *31*, 633–648.

[5] Inoue, A. Stabilization of metallic supercooled liquid and bulk amorphous alloys. *Acta Mater.* **2000**, *48*, 279–306.

[6] Tracy, C. L.; Park, S.; Rittman, D. R.; Zinkle, S. J.; Bei, H. B.; Lang, M.; Ewing, R. C.; Mao, W. L. High pressure synthesis of a hexagonal close-packed phase of the high-entropy alloy CrMnFeCoNi. *Nat. Commun.* **2017**, *8*, 15634.

[7] Liu, W. H.; Wu, Y.; He, J. Y.; Nieh, T. G.; Lu, Z. P. Grain growth and the Hall-Petch relationship in a high-entropy FeCrNiCoMn alloy. *Scr. Mater.* **2013**, *68*, 526–529.

[8] Lv, Z. Y.; Liu, X. J.; Jia, B.; Wang, H.; Wu, Y.; Lu, Z. P. Development of a novel high-entropy alloy with eminent efficiency of degrading azo dye solutions. *Sci. Rep.* **2016**, *6*, 34213.

[9] Egami, T. Atomic level stresses. *Prog. Mater. Sci.* **2011**, *56*, 637–653.

[10] Ranganathan, S. Alloyed pleasures: Multimetallic cocktails. *Curr. Sci.* **2003**, *85*, 1404–1406.

[11] Zhang, Z. J.; Mao, M. M.; Wang, J. W.; Gludovatz, B.; Zhang, Z.; Mao, S. X.; George, E. P.; Yu, Q.; Ritchie, R. O. Nanoscale origins of the damage tolerance of the high-entropy alloy CrMnFeCoNi. *Nat. Commun.* **2015**, *6*, 10143.

[12] Gludovatz, B.; Hohenwarter, A.; Catoor, D.; Chang, E. H.; George, E. P.; Ritchie, R. O. A fracture-resistant high-entropy alloy for cryogenic applications. *Science* **2014**, *345*, 1153–1158.

[13] Sauthoff, G. Multiphase intermetallic alloys for structural applications. *Intermetallics* **2000**, *8*, 1101–1109.

[14] Cantor, B. Multicomponent and high entropy alloys. *Entropy (Basel)* **2014**, *16*, 4749–4768.

[15] Otto, F.; Yang, Y.; Bei, H.; George, E. P. Relative effects of enthalpy and entropy on the phase stability of equiatomic high-entropy alloys. *Acta Mater.* **2013**, *61*, 2628–2638.

[16] Chang, X. J.; Zeng, M. Q.; Liu, K. L.; Fu, L. Phase engineering of high-entropy alloys. *Adv. Mater.* **2020**, *32*, 1907226.

[17] Sun, Y. F.; Dai, S. High-entropy materials for catalysis: A new frontier. *Sci. Adv.* **2021**, *7*, eabg1600.

[18] Jo, Y. H.; Jung, S.; Choi, W. M.; Sohn, S. S.; Kim, H. S.; Lee, B. J.; Kim, N. J.; Lee, S. Cryogenic strength improvement by utilizing room-temperature deformation twinning in a partially recrystallized VCrMnFeCoNi high-entropy alloy. *Nat. Commun.* **2017**, *8*, 15719.

[19] Cantor, B.; Chang, I. T. H.; Knight, P.; Vincent, A. J. B. Microstructural development in equiatomic multicomponent alloys. *Mater. Sci. Eng. A* **2004**, *375–377*, 213–218.

[20] Otto, F.; Dlouhý, A.; Somsen, C.; Bei, H.; Eggeler, G.; George, E. P. The influences of temperature and microstructure on the tensile properties of a CoCrFeMnNi high-entropy alloy. *Acta Mater.* **2013**, *61*, 5743–5755.

[21] Zhang, J. Y.; He, Q. F.; Li, J.; Yang, Y. Chemical fluctuation enabling strength-plasticity synergy in metastable single-phase high entropy alloy film with gigapascal yield strength. *Int. J. Plast.* **2021**, *139*, 102951.

[22] Lei, Y.; Hashimoto, N.; Isobe, S. Cu-containing high entropy alloys for nuclear fusion application. *Mater. Trans.* **2020**, *61*, 1247–1251.

[23] Sohn, S.; Liu, Y. H.; Liu, J. B.; Gong, P.; Prades-Rodel, S.; Blatter, A.; Scanley, B. E.; Broadbridge, C. C.; Schroers, J. Noble metal high entropy alloys. *Scr. Mater.* **2017**, *126*, 29–32.

[24] Qin, G.; Chen, R. R.; Zheng, H. T.; Fang, H. Z.; Wang, L.; Su, Y. Q.; Guo, J. J.; Fu, H. Z. Strengthening FCC-CoCrFeMnNi high entropy alloys by Mo addition. *J. Mater. Sci. Technol.* **2019**, *35*, 578–583.

[25] Naeem, M.; He, H. Y.; Zhang, F.; Huang, H. L.; Harjo, S.; Kawasaki, T.; Wang, B.; Lan, S.; Wu, Z. D.; Wang, F. et al. Cooperative deformation in high-entropy alloys at ultralow temperatures. *Sci. Adv.* **2020**, *6*, eaax4002.

[26] Ding, Q. Q.; Zhang, Y.; Chen, X.; Fu, X. Q.; Chen, D. K.; Chen, S. J.; Gu, L.; Wei, F.; Bei, H. B.; Gao, Y. F. et al. Tuning element distribution, structure and properties by composition in high-entropy

alloys. *Nature* **2019**, *574*, 223–227.
[27] Feng, R.; Feng, B. J.; Gao, M. C.; Zhang, C.; Neuefeind, J. C.; Poplawsky, J. D.; Ren, Y.; An, K.; Widom, M.; Liaw, P. K. Superior high-temperature strength in a supersaturated refractory high-entropy alloy. *Adv. Mater.* **2021**, *33*, 2102401.
[28] Li, R. X.; Qiao, J. W.; Liaw, P. K.; Zhang, Y. Preternatural hexagonal high-entropy alloys: A review. *Acta Metall. Sin. (Engl. Lett.)* **2020**, *33*, 1033–1045.
[29] Takeuchi, A.; Amiya, K.; Wada, T.; Yubuta, K.; Zhang, W. High-entropy alloys with a hexagonal close-packed structure designed by equi-atomic alloy strategy and binary phase diagrams. *JOM* **2014**, *66*, 1984–1992.
[30] Feuerbacher, M.; Heidelmann, M.; Thomas, C. Hexagonal high-entropy alloys. *Mater. Res. Lett.* **2015**, *3*, 1–6.
[31] Yusenko, K. V.; Bykova, E.; Bykov, M.; Riva, S.; Crichton, W. A.; Yusenko, M. V.; Sukhikh, A. S.; Arnaboldi, S.; Hanfland, M.; Dubrovinsky, L. S. et al. Ir-Re binary alloys under extreme conditions and their electrocatalytic activity in methanol oxidation. *Acta Mater.* **2017**, *139*, 236–243.
[32] Gao, M. C.; Zhang, B.; Guo, S. M.; Qiao, J. W.; Hawk, J. A. High-entropy alloys in hexagonal close-packed structure. *Metall. Mater. Trans. A* **2016**, *47*, 3322–3332.
[33] Rogal, L.; Ikeda, Y.; Lai, M. J.; Körmann, F.; Kalinowska, A.; Grabowski, B. Design of a dual-phase hcp-bcc high entropy alloy strengthened by ω nanoprecipitates in the Sc-Ti-Zr-Hf-Re system. *Mater. Des.* **2020**, *192*, 108716.
[34] Agrawal, P.; Shukla, S.; Gupta, S.; Agrawal, P.; Mishra, R. S. Friction stir gradient alloying: A high-throughput method to explore the influence of V in enabling HCP to BCC transformation in a γ-FCC dominated high entropy alloy. *Appl. Mater. Today* **2020**, *21*, 100853.
[35] Niu, C. N.; LaRosa, C. R.; Miao, J. S.; Mills, M. J.; Ghazisaeidi, M. Magnetically-driven phase transformation strengthening in high entropy alloys. *Nat. Commun.* **2018**, *9*, 1363.
[36] Zhang, F.; Wu, Y.; Lou, H. B.; Zeng, Z. D.; Prakapenka, V. B.; Greenberg, E.; Ren, Y.; Yan, J. Y.; Okasinski, J. S.; Liu, X. J. et al. Polymorphism in a high-entropy alloy. *Nat. Commun.* **2017**, *8*, 15687.
[37] Zhang, Y. Y.; Wu, H. B.; Yu, X. P.; Tang, D.; Yuan, R.; Sun, H. Microstructural evolution and strengthening mechanisms in $Cr_xMnFeNi$ high-entropy alloy. *J. Mater. Res. Technol.* **2021**, *12*, 2114–2127.
[38] Zhao, S. T.; Li, Z. Z.; Zhu, C. Y.; Yang, W.; Zhang, Z. R.; Armstrong, D. E. J.; Grant, P. S.; Ritchie, R. O.; Meyers, M. A. Amorphization in extreme deformation of the CrMnFeCoNi high-entropy alloy. *Sci. Adv.* **2021**, *7*, eabb3108.
[39] Jiang, L.; Hu, Y. J.; Sun, K.; Xiu, P.; Song, M.; Zhang, Y. W.; Boldman, W. L.; Crespillo, M. L.; Rack, P. D.; Qi, L. et al. Irradiation-induced extremes create hierarchical face-/body-centered-cubic phases in nanostructured high entropy alloys. *Adv. Mater.* **2020**, *32*, 2002652.
[40] Zhang, T.; Zhao, R. D.; Wu, F. F.; Lin, S. B.; Jiang, S. S.; Huang, Y. J.; Chen, S. H.; Eckert, J. Transformation-enhanced strength and ductility in a FeCoCrNiMn dual phase high-entropy alloy. *Mater. Sci. Eng. A* **2020**, *780*, 139182.
[41] Park, J. M.; Moon, J.; Bae, J. W.; Kim, D. H.; Jo, Y. H.; Lee, S.; Kim, H. S. Role of BCC phase on tensile behavior of dual-phase $Al_{0.5}CoCrFeMnNi$ high-entropy alloy at cryogenic temperature. *Mater. Sci. Eng. A* **2019**, *746*, 443–447.
[42] Liu, M.; Zuo, L.; Li, X.; Li, R.; Zhang, T. Microstructure and mechanical properties of $Al_{25-x}Cr_{25+0.5x}Fe_{25}Ni_{25+0.5x}$ (x=19, 17, 15 at.%) multi-component alloys. *Adv. Eng. Mater.* **2018**, *20*, 1701057.
[43] Zhang, Y.; Zhou, Y. J.; Lin, J. P.; Chen, G. L.; Liaw, P. K. Solid-solution phase formation rules for multi-component alloys. *Adv. Eng. Mater.* **2008**, *10*, 534–538.
[44] Fang, S. S.; Xiao, X. S.; Xia, L.; Li, W. H.; Dong, Y. D. Relationship between the widths of supercooled liquid regions and bond parameters of Mg-based bulk metallic glasses. *J. Non-Cryst. Solids* **2003**, *321*, 120–125.
[45] Guo, S.; Ng, C.; Lu, J.; Liu, C. T. Effect of valence electron concentration on stability of fcc or bcc phase in high entropy alloys. *J. Appl. Phys.* **2011**, *109*, 103505.
[46] Yang, X.; Zhang, Y. Prediction of high-entropy stabilized solid-solution in multi-component alloys. *Mater. Chem. Phys.* **2012**, *132*, 233–238.
[47] Tsai, K. Y.; Tsai, M. H.; Yeh, J. W. Sluggish diffusion in Co-Cr-Fe-Mn-Ni high-entropy alloys. *Acta Mater.* **2013**, *61*, 4887–4897.
[48] Ji, W.; Fu, Z. Y.; Wang, W. M.; Wang, H.; Zhang, J. Y.; Wang, Y. C.; Zhang, F. Mechanical alloying synthesis and spark plasma sintering consolidation of CoCrFeNiAl high-entropy alloy. *J. Alloys Compd.* **2014**, *589*, 61–66.
[49] Zhang, H.; Pan, Y.; He, Y. Z. Synthesis and characterization of FeCoNiCrCu high-entropy alloy coating by laser cladding. *Mater. Des.* **2011**, *32*, 1910–1915.
[50] Yue, T. M.; Xie, H.; Lin, X.; Yang, H. O.; Meng, G. H. Solidification behaviour in laser cladding of AlCoCrCuFeNi high-entropy alloy on magnesium substrates. *J. Alloys Compd.* **2014**, *587*, 588–593.
[51] Wang, X. Z.; Dong, Q.; Qiao, H. Y.; Huang, Z. N.; Saray, M. T.; Zhong, G.; Lin, Z. W.; Cui, M. J.; Brozena, A.; Hong, M. et al. Continuous synthesis of hollow high-entropy nanoparticles for energy and catalysis applications. *Adv. Mater.* **2020**, *32*, 2002853.
[52] Qiao, H. Y.; Saray, M. T.; Wang, X. Z.; Xu, S. M.; Chen, G.; Huang, Z. N.; Chen, C. J.; Zhong, G.; Dong, Q.; Hong, M. et al. Scalable synthesis of high entropy alloy nanoparticles by microwave heating. *ACS Nano* **2021**, *15*, 14928–14937.
[53] Yao, Y. G.; Huang, Z. N.; Xie, P. F.; Lacey, S. D.; Jacob, R. J.; Xie, H.; Chen, F. J.; Nie, A. M.; Pu, T. C.; Rehwoldt, M. et al. Carbothermal shock synthesis of high-entropy-alloy nanoparticles. *Science* **2018**, *359*, 1489–1494.
[54] Gao, S. J.; Hao, S. Y.; Huang, Z. N.; Yuan, Y. F.; Han, S.; Lei, L. C.; Zhang, X. W.; Shahbazian-Yassar, R.; Lu, J. Synthesis of high-entropy alloy nanoparticles on supports by the fast moving bed pyrolysis. *Nat. Commun.* **2020**, *11*, 2016.
[55] Joo, S. H.; Bae, J. W.; Park, W. Y.; Shimada, Y.; Wada, T.; Kim, H. S.; Takeuchi, A.; Konno, T. J.; Kato, H.; Okulov, I. V. Beating thermal coarsening in nanoporous materials via high-entropy design. *Adv. Mater.* **2020**, *32*, 1906160.
[56] Cai, Z. X.; Goou, H.; Ito, Y.; Tokunaga, T.; Miyauchi, M.; Abe, H.; Fujita, T. Nanoporous ultra-high-entropy alloys containing fourteen elements for water splitting electrocatalysis. *Chem. Sci.* **2021**, *12*, 11306–11315.
[57] Broge, N. L. N.; Bondesgaard, M.; Søndergaard-Pedersen, F.; Roelsgaard, M.; Iversen, B. B. Autocatalytic formation of high-entropy alloy nanoparticles. *Angew. Chem., Int. Ed.* **2020**, *59*, 21920–21924.
[58] Liu, M. M.; Zhang, Z. H.; Okejiri, F.; Yang, S. Z.; Zhou, S. H.; Dai, S. Entropy-maximized synthesis of multimetallic nanoparticle catalysts via a ultrasonication-assisted wet chemistry method under ambient conditions. *Adv. Mater. Interfaces* **2019**, *6*, 1900015.
[59] Okejiri, F.; Yang, Z. Z.; Chen, H.; Do-Thanh, C. L.; Wang, T.; Yang, S. Z.; Dai, S. Ultrasound-driven fabrication of high-entropy alloy nanocatalysts promoted by alcoholic ionic liquids. *Nano Res.* **2022**, *15*, 4792–4798.
[60] Wang, Y.; Mi, J. X.; Wu, Z. S. Recent status and challenging perspective of high entropy oxides for chemical catalysis. *Chem Catal.* **2022**, *2*, 1624–1656.
[61] Mateti, S.; Saranya, L.; Sathikumar, G.; Cai, Q. R.; Yao, Y. G.; Chen, Y. Nanomaterials enhancing the solid-state storage and decomposition of ammonia. *Nanotechnology* **2022**, *33*, 222001.
[62] Xie, P. F.; Yao, Y. G.; Huang, Z. N.; Liu, Z. Y.; Zhang, J. L.; Li, T. Y.; Wang, G. F.; Shahbazian-Yassar, R.; Hu, L. B.; Wang, C. Highly efficient decomposition of ammonia using high-entropy alloy catalysts. *Nat. Commun.* **2019**, *10*, 4011.
[63] Qiu, H. J.; Fang, G.; Wen, Y. R.; Liu, P.; Xie, G. Q.; Liu, X. J.; Sun, S. H. Nanoporous high-entropy alloys for highly stable and efficient

catalysts. *J. Mater. Chem. A* **2019**, *7*, 6499–6506.
[64] Mori, K.; Hashimoto, N.; Kamiuchi, N.; Yoshida, H.; Kobayashi, H.; Yamashita, H. Hydrogen spillover-driven synthesis of high-entropy alloy nanoparticles as a robust catalyst for CO_2 hydrogenation. *Nat. Commun.* **2021**, *12*, 3884.
[65] Ipadeola, A. K.; Lebechi, A. K.; Gaolatlhe, L.; Haruna, A. B.; Chitt, M.; Eid, K.; Abdullah, A. M.; Ozoemena, K. I. Porous high-entropy alloys as efficient electrocatalysts for water-splitting reactions. *Electrochem. Commun.* **2022**, *136*, 107207.
[66] Zhang, D.; Zhao, H.; Huang, B. L.; Li, B.; Li, H. D.; Han, Y.; Wang, Z. C.; Wu, X. K.; Pan, Y.; Sun, Y. J. et al. Advanced ultrathin RuPdM (M = Ni, Co, Fe) nanosheets electrocatalyst boosts hydrogen evolution. *ACS Cent. Sci.* **2019**, *5*, 1991–1997.
[67] Zhang, D.; Shi, Y.; Zhao, H.; Qi, W. J.; Chen, X. L.; Zhan, T. R.; Li, S. X.; Yang, B.; Sun, M. Z.; Lai, J. P. et al. The facile oil-phase synthesis of a multi-site synergistic high-entropy alloy to promote the alkaline hydrogen evolution reaction. *J. Mater. Chem. A* **2021**, *9*, 889–893.
[68] Yao, R. Q.; Zhou, Y. T.; Shi, H.; Wan, W. B.; Zhang, Q. H.; Gu, L.; Zhu, Y. F.; Wen, Z.; Lang, X. Y.; Jiang, Q. Nanoporous surface high-entropy alloys as highly efficient multisite electrocatalysts for nonacidic hydrogen evolution reaction. *Adv. Funct. Mater.* **2021**, *31*, 2009613.
[69] Sharma, L.; Katiyar, N. K.; Parui, A.; Das, R.; Kumar, R.; Tiwary, C. S.; Singh, A. K.; Halder, A.; Biswas, K. Low-cost high entropy alloy (HEA) for high-efficiency oxygen evolution reaction (OER). *Nano Res.* **2022**, *15*, 4799–4806.
[70] Qiu, H. J.; Fang, G.; Gao, J. J.; Wen, Y. R.; Lv, J.; Li, H. L.; Xie, G. Q.; Liu, X. J.; Sun, S. H. Noble metal-free nanoporous high-entropy alloys as highly efficient electrocatalysts for oxygen evolution reaction. *ACS Mater. Lett.* **2019**, *1*, 526–533.
[71] Wang, A. L.; Wan, H. C.; Xu, H.; Tong, Y. X.; Li, G. R. Quinary PdNiCoCuFe alloy nanotube arrays as efficient electrocatalysts for methanol oxidation. *Electrochim. Acta* **2014**, *127*, 448–453.
[72] Li, H. D.; Han, Y.; Zhao, H.; Qi, W. J.; Zhang, D.; Yu, Y. D.; Cai, W. W.; Li, S. X.; Lai, J. P.; Huang, B. L. et al. Fast site-to-site electron transfer of high-entropy alloy nanocatalyst driving redox electrocatalysis. *Nat. Commun.* **2020**, *11*, 5437.
[73] Wu, D. S.; Kusada, K.; Yamamoto, T.; Toriyama, T.; Matsumura, S.; Kawaguchi, S.; Kubota, Y.; Kitagawa, H. Platinum-group-metal high-entropy-alloy nanoparticles. *J. Am. Chem. Soc.* **2020**, *142*, 13833–13838.
[74] Nellaiappan, S.; Katiyar, N. K.; Kumar, R.; Parui, A.; Malviya, K. D.; Pradeep, K. G.; Singh, A. K.; Sharma, S.; Tiwary, C. S.; Biswas, K. High-entropy alloys as catalysts for the CO_2 and CO reduction reactions: experimental realization. *ACS Catal.* **2020**, *10*, 3658–3663.
[75] Araujo, R. B.; Pehlivan, I. B.; Edvinsson, T. High-entropy alloy catalysts: Fundamental aspects, promises towards electrochemical NH_3 production, and lessons to learn from deep neural networks. *Nano Energy* **2023**, *105*, 108027.
[76] Zhang, D.; Zhao, H.; Wu, X. K.; Deng, Y.; Wang, Z. C.; Han, Y.; Li, H. D.; Shi, Y.; Chen, X. L.; Li, S. X. et al. Multi-site electrocatalysts boost pH-universal nitrogen reduction by high-entropy alloys. *Adv. Funct. Mater.* **2021**, *31*, 2006939.
[77] Li, R. X.; Xie, L.; Wang, W. Y.; Liaw, P. K.; Zhang, Y. High-throughput calculations for high-entropy alloys: A brief review. *Front. Mater.* **2020**, *7*, 575852.
[78] Feng, R.; Zhang, C.; Gao, M. C.; Pei, Z. R.; Zhang, F.; Chen, Y.; Ma, D.; An, K.; Poplawsky, J. D.; Ouyang, L. Z. et al. High-throughput design of high-performance lightweight high-entropy alloys. *Nat. Commun.* **2021**, *12*, 4329.



Xiaoxiao Han received her BSc degree from Northeast Normal University in 2021. Currently, she is studying for a master's degree under the guidance of Prof. Hongjie Zhang at the Changchun Institute of Applied Chemistry, Chinese Academy of Science. Her research interests involve the synthesis of rare earth-based heterogeneous catalysts



Lingling Zhang received her BSc and PhD from Jilin University in 2017 and 2022 respectively. She is currently working under the direction of Prof. Xiao Wang at Changchun Institute of Applied Chemistry, CAS. Her research interests focus on the preparation of rare earth-based heterogeneous catalysts



Shuyan Song received his BSc degree in Chemistry in 2003 and MSc in inorganic chemistry in 2006 both from Northeast Normal University. He joined the group of Prof. Hongjie Zhang at Changchun Institute of Applied Chemistry, Chinese Academy of Sciences (CAS), where he received his PhD in inorganic chemistry in 2009. He is working as a professor under the direction of Prof. Zhang at Changchun Institute of Applied Chemistry, CAS. His research focus is primarily on the development of porous functional materials for heterogeneous catalysis, proton conduction, chemical sensing and detection



Hongjie Zhang received his BSc degree from Peking University in 1978. He then worked as a research assistant in Changchun Institute of Applied Chemistry, where he received his MSc degree in Inorganic Chemistry in 1985. Then, he worked as an assistant professor at the same institute from 1985–1989. He then studied at Universite de Bordeaux I, Laboratoire de Chimie du Solide du CNRS (France), where he received his PhD degree in Solid State Chemistry and Materials Sciences in 1993. He joined Changchun Institute of Applied Chemistry, CAS, as a professor in 1994. His current research interests include lanthanide organic-inorganic hybrid materials, electroluminescent devices, functional nanomaterials, and the structure and properties of rare earth magnesium alloys